JACS
JOURNAL OF THE AMERICAN CHEMICAL SOCIETY

Article

pubs.acs.org/JACS

New Roles for Icosahedral Clusters in Intermetallic Phases: Micelle-like Segregation of Ca−Cd and Cu−Cd Interactions in $Ca_{10}Cd_{27}Cu_2$

Amelia B. Hadler, Nicholas A. Harris, and Daniel C. Fredrickson*

Department of Chemistry, University of Wisconsin—Madison, 1101 University Avenue, Madison, Wisconsin 53706, United States

Supporting Information

ABSTRACT: Despite significant progress in the structural characterization of the quasicrystalline state, the chemical origins of long- and short-range icosahedral order remain mysterious and a subject of debate. In this Article, we present the crystal structure of a new complex intermetallic phase, $Ca_{10}Cd_{27}Cu_2$ (*mC*234.24), whose geometrical features offer clues to the driving forces underlying the icosahedral clusters that occur in Bergman-type quasicrystals. $Ca_{10}Cd_{27}Cu_2$ adopts a *C*-centered monoclinic superstructure of the 1/1 Bergman approximant structure, in which [110] layers of Bergman clusters in the 1/1 structure are separated through the insertion of additional atoms (accompanied by substantial positional disorder). An examination of the coordination environments of Ca and Cu (in the ordered regions) reveals that the structure can be viewed as a combination of coordination polyhedra present in the nearest binary phases in the Ca−Cd−Cu compositional space. A notable feature is the separation of Ca−Cd and Cu−Cd interactions, with Bergman clusters emerging as Ca−Cd Friauf polyhedra (derived from the $MgZn_2$-type $CaCd_2$ phase) encapsulate a Cu−Cd icosahedron similar to those appearing in Cu_2Cd_5. DFT chemical pressure calculations on nearby binary phases point to the importance of this segregation of Ca−Cd and Cu−Cd interactions. The mismatch in atomic size between Cu and Cd leads to an inability to satisfy Ca−Cu and Ca−Cd interactions simultaneously in the Friauf polyhedra of the nearby Laves phase $CaCd_2$. The relegation of the Cu atoms to icosahedra prevents this frustration while nucleating the formation of Bergman clusters.

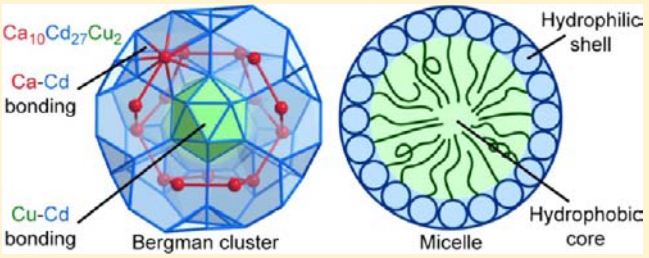

1. INTRODUCTION

Quasicrystals are phases of condensed matter that exhibit the sharp diffraction peaks normally associated with lattice periodicity, but arrayed in symmetries incompatible with such periodicity: icosahedral, decagonal, dodecagonal, and octagonal.[1] The study of quasicrystals has undergone staggering growth since the first icosahedral diffraction patterns of rapidly cooled alloys shook the foundations of crystallography in 1984.[2] The crystallographic theory, structure solution, and refinement of icosahedral and decagonal quasicrystals have been developed,[3−7] and quasicrystallinity has been shown to extend beyond the realm of metals and alloys. Dodecagonal phases and related structures have emerged in such systems as micelle-forming dendrimers,[8] block copolymers,[9−11] colloidal nanoparticles,[12] and MD simulations using monatomic spheres,[13,14] and proposals have been made for the design of organic quasicrystals from molecular units.[15−17]

And yet, fundamental and alluring questions remain: the driving forces underlying the formation of quasicrystals are still the subject of debate.[18] Intermetallic quasicrystals are generally regarded as Hume−Rothery phases, with the valence electron concentration being an important factor governing stability.[19−23] For icosahedral quasicrystals, this view is confirmed by the correlation between preferred electron counts and pseudogaps in the electronic density of states (DOS) curves at the Fermi energy.[24−26] Tuning the electron count of a related phase such as Mg_2Zn_{11} to reach a pseudogap has been shown to produce new icosahedral quasicrystals and approximants.[27−30] Atomic sizes are also known empirically to play a role,[22,31−33] but the ways in which these factors work together to determine a quasicrystal's structure remain mysterious.

The observation of quasicrystalline arrangements beyond intermetallics might cause one to wonder if more general themes are at work in these phases. Could the parallels between the quasicrystals of intermetallics and soft materials reflect analogous driving forces shaping their structures? Indeed, minimal surfaces and the similar periodic nodal surfaces have been widely used as organizing principles in discussing the crystal structures of inorganic compounds.[34−39] Electronic structure calculations in a few intermetallics have confirmed that these surfaces can represent transitions between regions of differing bonding modes.[40,41] These surfaces recall the minimization of interfacial area between poorly miscible domains as in block copolymers and micelles.[42,43]

Such connections between structural complexity and the coexistence of mutually exclusive bonding or packing modes are increasingly being recognized in intermetallic systems. Our interest in this notion has led us to perform exploratory synthesis in ternary systems in which incompatibilities arise

Received: July 16, 2013
Published: October 22, 2013

   dx.doi.org/10.1021/ja407291t | J. Am. Chem. Soc. 2013, 135, 17369−17378

between the preferred bonding types of the binary subsystems. Ternary phases in such systems would then be forced to reconcile these conflicts, which we term chemical frustration by analogy to magnetic phenomena.[44,45] One candidate that we identified is the Ca−Cd−Cu system, in which we envisioned the tetrahedral close-packed ordering of the Cu−Cd phases as conflicting with the tendency of Ca to agglomerate into domains of simple close-packing in Ca-rich Ca−Cu and Ca−Cd compounds.[44]

In this Article, we describe the crystal structure of a complex intermetallic phase emerging from our synthetic explorations of the Ca−Cd−Cu system, $Ca_{10}Cd_{27}Cu_2$, which illustrates how local icosahedral order can emerge from chemical frustration. $Ca_{10}Cd_{27}Cu_2$ crystallizes in a new ternary structure type based on Bergman clusters (Figure 1), a fundamental motif in

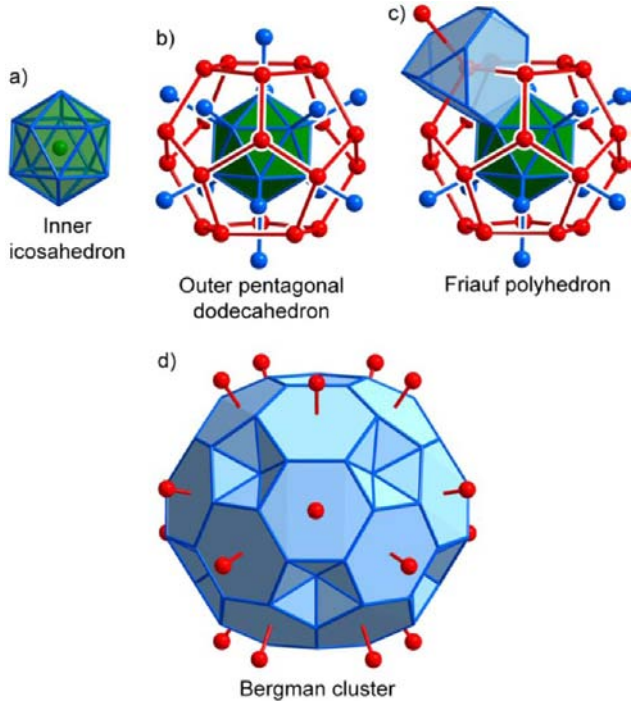

Figure 1. Bergman-type cluster. The Bergman cluster's center is (a) an icosahedron, with or without a central atom. This is surrounded by (b) a pentagonal dodecahedron, each atom of which is coordinated to (c) a Friauf polyhedron, thus creating (d) the full cluster.

Bergman-type quasicrystals.[46] The prevalence of Bergman clusters in this structure is surprising, because Ca/Cd-based intermetallics are better known for the Tsai-type quasicrystal $CaCd_{5.7}$[7,47] and its approximants $CaCd_6$[48] and $Ca_{13}Cd_{76}$.[49] As we will see in this Article, the stability of the Bergman clusters is traceable to their ability to allow the spatial segregation of Ca−Cd and Cd−Cu interactions. The Bergman clusters in this compound then represent an encapsulation of one bonding type with another in a manner reminiscent of micelles formed by amphiphilic molecules.[43]

2. TECHNICAL PROCEDURES

2.1. Synthesis. $Ca_{10}Cd_{27}Cu_2$ was synthesized from the pure elements (cadmium, Strem Chemicals, 99.999%, granules 1−5 mm, cut to size with wire cutters; calcium, Alfa Aesar, 99.5%, redistilled granules −16 mesh; copper, Alfa Aesar, 99.5%, powder −150 mesh). The elements were weighed out in stoichiometric ratios in an Ar-filled glovebox and placed into 0.5-cm-diameter Ta tubes, which were welded shut and sealed in evacuated fused silica ampoules. To obtain samples with the highest possible phase purity for powder X-ray diffraction and elemental analysis, the ampoules were heated to 1100 °C in a muffle furnace for 48 h, quenched in an ice−water bath, and annealed at 500 °C for 100 h. To optimize single-crystal formation, the ampoules were heated to 1100 °C in a muffle furnace for 48 h, cooled to 500 °C at a rate of 5 °C/h, and subsequently annealed for 6 days. All syntheses resulted in brittle, shiny gray pieces that showed minimal air sensitivity, with noticeable oxidation occurring only after months in air.

2.2. Phase Analysis with Powder X-ray Diffraction. Powder X-ray diffraction data was collected on a Bruker D8 ADVANCE diffractometer with Cu Kα radiation (λ = 1.54051 Å). Qualitative comparison to a calculated powder pattern for $Ca_{10}Cd_{27}Cu_2$ suggested that $Ca_{10}Cd_{27}Cu_2$ was the major phase present when the samples were quenched from 1100 °C then annealed. See the Supporting Information for further details.

2.3. Elemental Analysis with Energy-Dispersive X-ray Spectroscopy (EDS). Uncrushed pieces of the sample were suspended in epoxy, hand-polished against diamond lapping films, and polished further with a 0.25 μm diamond suspension on a diamond wheel. The polished samples were then carbon coated and examined with a Hitachi S-3100N scanning electron microscope equipped with an EDS probe (voltage = 15 kV). An analysis of the sample revealed a major phase with composition $Ca_{9.27(17)}Cd_{26.7(2)}Cu_{2.19(27)}$ as well as a Cd-rich minor phase, likely $Ca_2Cu_2Cd_9$ and/or $Ca_{14}Cd_{51}$. No substantial impurities heavier than sodium were observed.

2.4. Single-Crystal X-ray Diffraction Measurements. Several irregularly shaped single crystals were picked from uncrushed samples. Initial X-ray diffraction measurements were performed on an Agilent Technologies Xcalibur E diffractometer with a Mo Kα sealed-tube X-ray source, and processing of the frame data was performed with program CrysalisPro, ver. 171.[50] The final data set was collected on a Bruker Quazar APEX2 diffractometer with a Mo Kα IμS microfocus X-ray source. The run list involved ω scans and φ scans with a step size of 0.50 chosen to cover a sphere of reciprocal space up to a resolution of 0.60 Å. Processing of the frame data was performed with the APEX2 software suite[51] and with the program XPREP.[52] Further details can be found in Table 1.

2.5. Structure Solution and Refinement. An inspection of reciprocal lattice reconstructions from frame data revealed systematic absences suggesting a *C*-centered space group in Laue class 2/*m*. Data reduction was performed assuming the space group *C*2/*m* (or a possible subgroup), and the successful structural solution supports the choice of *C*2/*m*. The charge-flipping algorithm,[54,55] as implemented in the program SUPERFLIP,[56] was used to obtain a starting model for this phase, yielding 39 symmetry-distinct sites in a 236-atom unit cell.

The refinement of the model against the data was performed in Jana2006 on F^2.[57] Three-dimensional electron density reconstructions were visualized using the program VESTA.[58] The resulting structural solution showed significant structural and chemical disorder in 11 of the 39 crystallographic sites. Full details of the site modeling process can be found in the Supporting Information; a brief overview of the modeling approach is given below.

The disordered region is centered on partially occupied copper site Cu3a. Six surrounding sites (Ca6a/b, Ca9a/b, Cd19a/b, Cd20a/b, Cu4a/b, and Cu5a/b) were modeled as a split between two spatially distinct atomic locations; the *a* sites were considered to be present when Cu3a was occupied whereas the *b* sites were occupied otherwise. The restrained occupancies converged to 56.08(11)% for the *a* sites, with 43.92(11)% occupancy for the *b* sites. Four other sites (Ca10, Cd22, Cd23, and Cd24) also showed positional or compositional disorder. The Ca10 site was modeled as a Ca/Cd split site with 79.95(18)% calcium and 20.05(18)% cadmium. The Cd22, Cd23, and Cd24 sites were refined independently as having mixed occupation with copper. All positionally disordered sites were consistent between different crystals, with only minor changes in positions, occupancies, and displacement parameters.

Upon switching to an anisotropic refinement for all sites lacking positional disorder, the R($I > 3\sigma$) value converged to 2.84 (Table 1).

dx.doi.org/10.1021/ja407291t | J. Am. Chem. Soc. 2013, 135, 17369−17378

Table 1. Crystal Data for $Ca_{10}Cd_{27}Cu_2$[a]

chemical formula	$Ca_{10.40}Cd_{26.71}Cu_{1.94}$
Pearson symbol	*m*C234.24
EDS composition	$Ca_{9.27(17)}Cd_{26.7(2)}Cu_{2.19(27)}$[b]
space group	*C*2/*m* (No. 12)
a (Å)	22.7005(6)
b (Å)	15.5829(4)
c (Å)	16.2015(4)
β (deg)	104.3959(14)
cell volume (Å^3), calcd density (g/cm^3)	5551.2(3), 6.3545
crystal dimensions (mm^3)	0.054 × 0.038 × 0.036
crystal color	metallic gray
data collection temperature	room temperature
radiation source, λ (Å)	Mo Kα, 0.7107
absorption coeff (mm^{-1}), correction	17.486, analytical[53]
minimum, maximum transmission	0.5502, 0.7459
θ_{min}, θ_{max}	1.3, 36.49
number of reflections	193 527
unique reflections (all, $I > 3\sigma$)	13 968, 10 077
R_{int} (all, $I > 3\sigma$)	5.72, 4.99
number of parameters	290
R ($I > 3\sigma$), R_w ($I > 3\sigma$)	2.84, 5.62
R(all), R_w(all)	5.07, 6.18
S ($I > 3\sigma$), S(all)	1.37, 1.27
$\Delta\rho_{max}$, $\Delta\rho_{min}$ (electrons/Å^3)	4.92[c], −3.85[c]

[a]A crystallographic information file containing further details can be obtained from the Fachinformationszentrum Karlsruhe (e-mail: crysdata@fiz-karlsruhe.de) on quoting depository number 426438. [b]The discrepancy between the crystallographically refined Ca content and the Ca content from EDS in the bulk sample can be attributed to a combination of the semiquantitative nature of the EDS results and the difficulty of achieving unambiguous site assignments in the disordered region. [c]The maximum and minimum are respectively 0.59 Å from Ca10a and 0.21 Å from Cu5b, both of which show positional disorder; see Figure S2c for a detailed map.

All interatomic distances were found to be consistent with the atomic identities assigned to the sites. The largest peaks in the Fourier difference map were 4.92 and −3.85 electrons/Å^3 and are associated with the positional disorder. Further details, including tables of the refined atomic coordinates, atomic displacement parameters, and interatomic distances, are given in the Supporting Information.

2.6. Electronic Structure Calculations. DFT-CP analyses were performed on a series of structures related to that of $Ca_{10}Cd_{27}Cu_2$: $MgZn_2$-type $CaCd_2$, derivatives of $CaCd_2$ with one Cu atom/unit cell placed on either the Cd1 or Cd2 sites, and Cu_2Cd_5 (Co_2Al_5 type). The structures were first geometrically optimized using LDA-DFT as implemented in either the ABINIT[59−62] or VASP[63−65] packages. Single-point calculations were then carried out with ABINIT on the optimized structures as well as on slightly expanded and contracted unit cells for a total volume range of 0.6%. For each geometry, the total Kohn−Sham potential, Hartree potential, kinetic energy density, and electron density were output on voxel grids. The grid data was used as input for the generation of CP maps with CPcalc_abinit.[66,67] Isotropic core averaging was applied to the CP map with the core radii set to 85% of the metallic radii of the corresponding elements. The CP map was integrated using the contact volume scheme with CPintegrate.[67] Full details of the pseudopotentials, k-point meshes, and energy cutoffs used as well as the optimized geometries, total energies, and issues encountered during the CP analysis may be found in the Supporting Information.

3. RESULTS AND DISCUSSION

3.1. Crystal Structure of $Ca_{10}Cd_{27}Cu_2$. $Ca_{10}Cd_{27}Cu_2$ crystallizes in a complex *C*-centered monoclinic unit cell with 39 symmetry-inequivalent atomic sites for a total of 272 atomic positions/unit cell (which reduces to 234.24 atoms/unit cell when partial occupations are considered). The visualization of the crystal structure is greatly aided by the recognition of Bergman clusters at the lattice points of the *m*C Bravais lattice. The compositional makeup and spatial arrangement of the Bergman clusters here are closely related to those of the 1/1 Bergman-type quasicrystal approximant structures, as exemplified by $Na_{13}(Cd,Tl)_{27}$.[68]

For both $Ca_{10}Cd_{27}Cu_2$ and $Na_{13}(Cd,Tl)_{27}$, the truncated tetrahedral (TT) networks of the Friauf polyhedra serve as sites for the relatively electronegative Cd or Cd/Tl atoms, whereas diamondoid (D) sites threading through the TT network are predominantly occupied by the electropositive Ca or Na atoms. In $Ca_{10}Cd_{27}Cu_2$, minor Cu substitution occurs on some of the TT sites, whereas a few of the D sites exhibit mixed Ca/Cd or Cd occupancy. A more pronounced difference between the Bergman clusters of these two phases is found in their interiors: in $Na_{13}(Cd,Tl)_{27}$ the central icosahedron is empty, but in $Ca_{10}Cd_{27}Cu_2$ it is occupied by a Cu atom.

The uniqueness of the $Ca_{10}Cd_{27}Cu_2$ structure is more apparent in comparing the packing of its Bergman clusters with that of $Na_{13}(Cd,Tl)_{27}$. In $Na_{13}(Cd,Tl)_{27}$, the clusters pack to form a simple I-centered lattice (Figure 2a,b). A similar body-centered packing can be seen in $Ca_{10}Cd_{27}Cu_2$, particularly when transforming it into a nonstandard I-centered setting, as is done in Figure 2d,e. However, differences appear in how the clusters are joined with their neighbors. Whereas in $Na_{13}(Cd,Tl)_{27}$ each Bergman cluster shares hexagonal faces with its eight nearest neighbors positioned at the corners of a cube, in the more complex $Ca_{10}Cd_{27}Cu_2$ structure only four of these connections remain intact (Figure 2a,d, green bars). The retained connections all lie within the [−101] family of planes. As such, the 3D array of face-sharing Bergman clusters seen in $Na_{13}(Cd,Tl)_{27}$ is reduced to 2D layers of these clusters in $Ca_{10}Cd_{27}Cu_2$. In the process, the cubic symmetry of the former structure is lowered to the monoclinic symmetry of the latter.

At this point, we have already accounted for 34 of the 39 symmetry-distinct atomic positions in the $Ca_{10}Cd_{27}Cu_2$ structure. To locate the remaining atoms, it is more straightforward to move back to the conventional *C*-centered monoclinic unit cell (Figure 3). In this setting, the Bergman layers now lie in the *ab* planes of the structure, with interstitial atoms filling the resulting space along *c*.

Figure 3a shows a Bergman cluster layer viewed down *c*. The remaining atoms are associated with three polyhedra (shown below the Bergman layer in Figure 3a) that decorate this layer. The first is a Friauf polyhedron centered on the Ca8 site. This Friauf polyhedron is distinct in that three of the four diamondoid network sites are occupied by Cd (blue) rather than Ca atoms, to resemble the expected coordination in an $AuBe_5$-type phase.[69] The second is derived from the μ-phase polyhedron but is subject to significant positional and compositional disorder, which includes its central Ca9 site. The final polyhedron is an icosahedron centered on the Cu2 site.

Each polyhedron fuses to the Bergman layer through shared faces, as is highlighted through color coding in Figure 3a. The Friauf (light blue) and μ-phase (orange) polyhedra occupy gaps within the Bergman cluster layers, with four sites directed into the interstitial layer: two of the Cd-occupied D sites in the Friauf polyhedron and two disordered Cu and Cd sites in the μ-

dx.doi.org/10.1021/ja407291t | J. Am. Chem. Soc. 2013, 135, 17369−17378

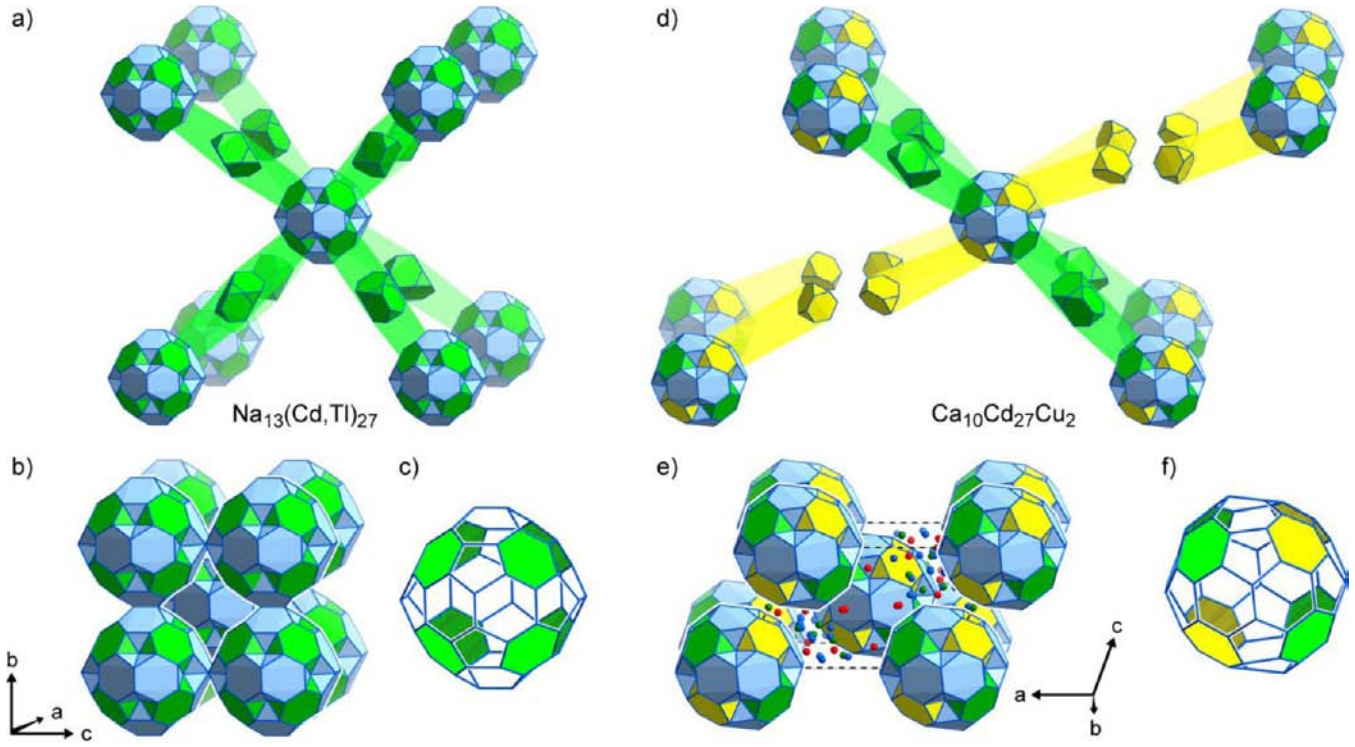

Figure 2. Packing of Bergman clusters in the related structures of $Na_{13}(Cd,Tl)_{27}$ and $Ca_{10}Cd_{27}Cu_2$. $Na_{13}(Cd,Tl)_{27}$ is built from (a) Bergman clusters that share hexagonal faces, forming (b) a cubic *I*-centered array. (c) Each cluster shares eight hexagonal faces (green) with its neighbors. An *I*-centered setting of the monoclinic $Ca_{10}Cd_{27}Cu_2$ structure shows (d) a plane of face-sharing Bergman clusters (green) with interrupted connections (yellow) to the neighboring planes. (e) The interstitial space between Bergman planes is filled with additional atoms (Cd, blue; Cu, green; Ca, red) in the full unit cell. (f) Each Bergman cluster in $Ca_{10}Cd_{27}Cu_2$ shares only four faces (green) with neighboring clusters.

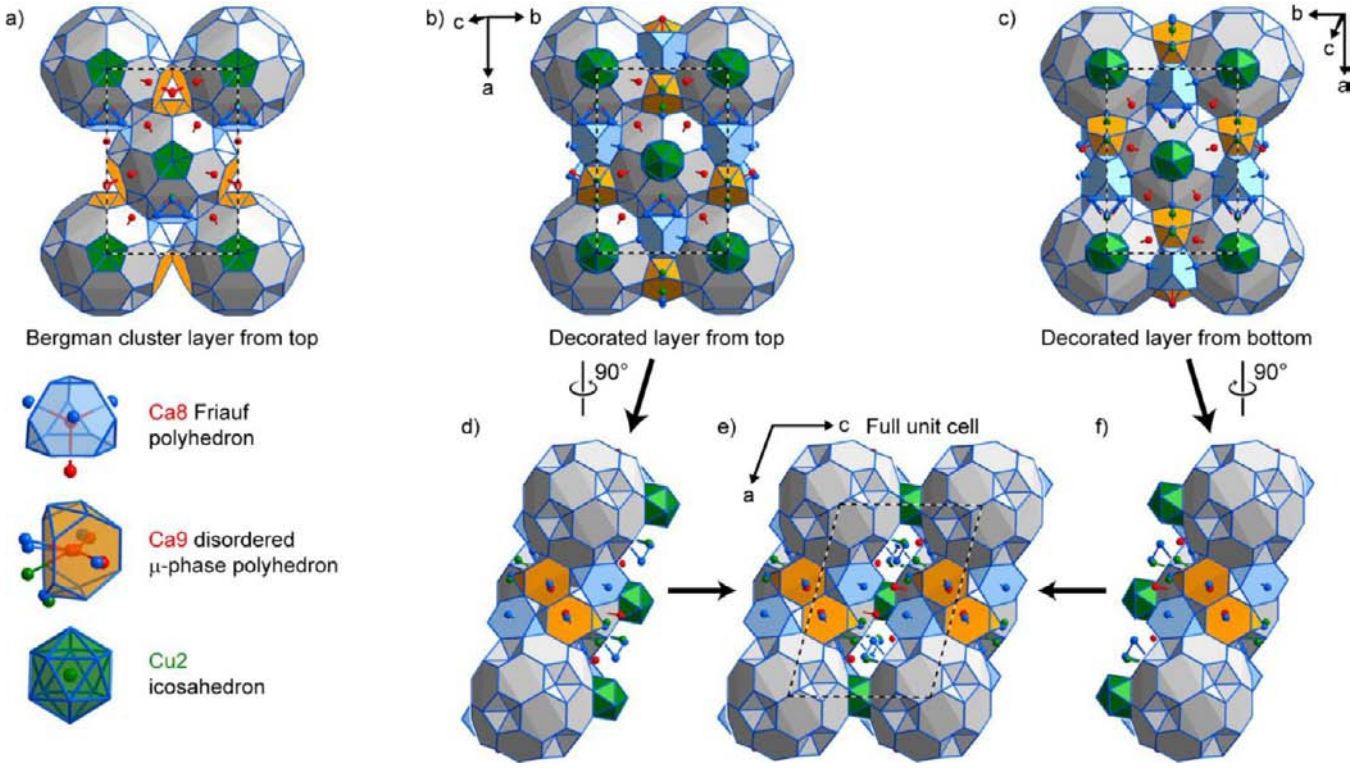

Figure 3. The complete structure of $Ca_{10}Cd_{27}Cu_2$. (a) One *C*-centered layer of Bergman clusters is shown from the top. Cluster faces shared with additional polyhedra are colored correspondingly. Bergman layers fully decorated with these additional polyhedra are shown (b, c) and rotated and fused (d, f) to form (e) the full unit cell of $Ca_{10}Cd_{27}Cu_2$, with all atoms accounted for.

dx.doi.org/10.1021/ja407291t | *J. Am. Chem. Soc.* 2013, 135, 17369−17378

phase polyhedron. The icosahedra (green) fit into pentagons on the top and bottom of the Bergman clusters.

The layers decorated with these polyhedra are shown from above and below the *ab* plane, respectively, in Figure 3b,c. The full structure can be constructed by rotating these decorated planes toward each other as if closing a sandwich (Figure 3d,f) and joining them through shared icosahedra (Figure 3e). The Bergman clusters linked by icosahedra are related by cell translations along *c*.

We have now accounted for all atoms in the unit cell of $Ca_{10}Cd_{27}Cu_2$ but have mentioned only briefly the profound disorder that it contains. Most of the disorder is localized within a region between two Bergman clusters (shown in Figure 4a) which contains the μ-phase polyhedron introduced in Figure 3a. The disorder centers around the partially occupied Cu3a site (occupancy = 56%). The fractional occupancy of this site leads to elongated density distributions around the neighboring sites (Figure 4c), suggesting that these positions adjust to the presence or absence of a Cu3a atom. Six of Cu3a's neighboring sites are thus affected: Ca6, Ca9, Cu4, Cu5, Cd19, and Cd20 (Figure 4b). Each of these are modeled as being split between two possible positions, labeled *a* and *b*, which are occupied when a Cu3a atom is present and absent, respectively. The structural response to the Cu3a occupation/vacancy includes the composition of the Cu4a/b and Cu5a/b sites, in which both *a* sites are occupied by Cu, whereas both *b* sites are occupied by Cd.

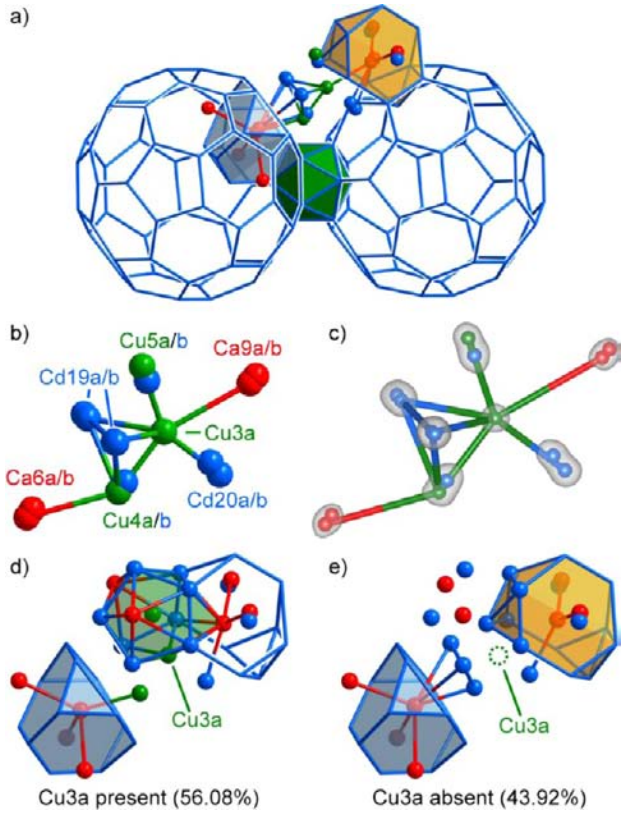

Figure 4. Positional disorder in $Ca_{10}Cd_{27}Cu_2$. The major disorder is localized between (a) two Bergman cluster layers, where (b) partial occupation of the Cu3a site causes positional disorder in six additional sites. (c) Electron density map showing elongated densities surrounding these sites. (d) When Cu3a is occupied, a distorted icosahedron forms around Cu5a. (e) When Cu3a is not occupied, no such icosahedron is present.

The presence or absence of Cu3a has implications for the structural description of the phase as well. When Cu3a and the resulting *a* sites are present, Cu5a centers a slightly distorted icosahedron, drawn in green in Figure 4d. When Cu3a is absent, no such icosahedron can be drawn around Cu5b, which is now a Cd site (Figure 4e). Cu3a's presence thus creates an icosahedron that can be filled by an additional Cu atom, increasing the amount of Cu that the structure can accommodate and emphasizing Cu's preference for Cd-rich icosahedra.

In summary, the crystal structure of $Ca_{10}Cd_{27}Cu_2$ can be viewed as being derived from the 1/1 Bergman quasicrystal approximant structure of $Na_{13}(Cd,Tl)_{27}$. We begin with the body-centered packing of face-sharing Bergman clusters of the 1/1 approximant and slice it into layers of these clusters along the [−101] planes. These layers are then stacked so that Bergman clusters of neighboring layers lie directly above each other. Where the outer pentagonal faces of the Bergman clusters meet between neighboring layers, a Cu atom is placed (Cu2) that acquires icosahedral coordination. Additional atoms, as well as some disorder, are found in the remaining space.

3.2. Structure−Composition Space Analysis. As we saw in the previous section, a dominant structural motif in the $Ca_{10}Cd_{27}Cu_2$ structure is the Bergman cluster. The presence of these icosahedral clusters in a Ca−Cd-based phase is somewhat surprising: the Ca−Cd system is well known for its Tsai-type quasicrystal and approximant structures, in which Tsai-type clusters are prevalent. The remaining phases in the Ca−Cd binary phase diagram, like all of the compounds in the Ca−Cu and Cu−Cd systems, show little relation to quasicrystals.[48] Evidently, the introduction of a small amount of Cu into a Ca−Cd mixture has led to the stabilization of Bergman clusters.

As in the Ca_5Cu_2Cd and $Ca_2Cu_2Cd_9$ compounds we described in an earlier work,[44] the structural features of $Ca_{10}Cd_{27}Cu_2$ (including its Bergman clusters) can be largely rationalized by the phase's position in the composition space of the Ca−Cd−Cu phase diagram (Figure 5). The formula $Ca_{10}Cd_{27}Cu_2$ sits just off the Ca−Cd edge, almost equidistant to $CaCd_2$ ($MgZn_2$-type at room temperature)[70] and $Ca_{14}Cd_{51}$ ($Gd_{14}Ag_{51}$-type).[48] It is intermediate in composition between these Ca−Cd phases and the Cu_2Cd_5 (Co_2Al_5-type)[71] phase on the Cu−Cd edge: $Ca_{10.4}Cd_{26.7}Cu_{1.9}$ = 9.70 $CaCd_2$ + 0.95 Cu_2Cd_5 + 0.05 $Ca_{14}Cd_{51}$.

In all of these binary phases, Cd serves as the majority element whose sublattice is structured to accommodate the Ca or Cu atoms. The resulting coordination polyhedra of the Ca and Cu closely resemble those in $Ca_{10}Cd_{27}Cu_2$ (Figure 5). For example, the Ca atoms in $CaCd_2$ are coordinated by Ca_4Cd_{12} Friauf polyhedra, just as are a majority of the Ca atoms in the dodecahedral shells of the Bergman clusters in $Ca_{10}Cd_{27}Cu_2$. Likewise, the Ca9 disordered μ-phase polyhedron in $Ca_{10}Cd_{27}Cu_2$ bears similarities to one of the Ca coordination environments in $Ca_{14}Cd_{51}$, which can be built from adding one vertex to a μ-phase polyhedron. Finally, the Cd_{12} icosahedral coordination (with minor Cu substitution) around the fully occupied Cu atoms in $Ca_{10}Cd_{27}Cu_2$ mirrors similar icosahedra in Cu_2Cd_5.

For each of these polyhedra, Ca−Cd and Cu−Cd interactions dominate; at least in the ordered portions of $Ca_{10}Cd_{27}Cu_2$ little driving force for Ca−Cu contacts is apparent. Taking these observations together, the expression

dx.doi.org/10.1021/ja407291t | J. Am. Chem. Soc. 2013, 135, 17369−17378

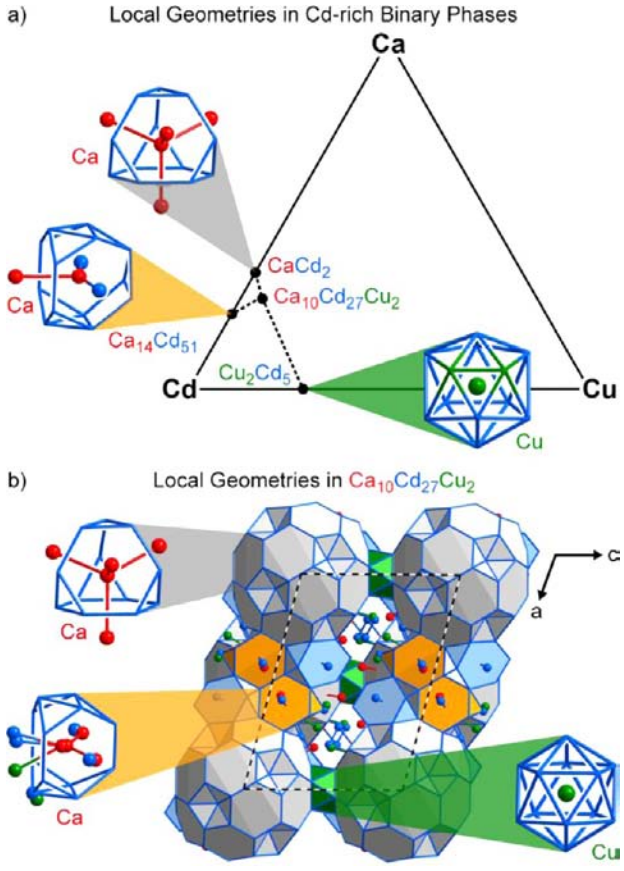

Figure 5. Structure−composition space analysis of $Ca_{10}Cd_{27}Cu_2$. (a) $Ca_{10}Cd_{27}Cu_2$'s position in the Ca−Cd−Cu phase diagram makes its composition a linear combination of those of binary phases $CaCd_2$, $Ca_{14}Cd_{51}$, and Cu_2Cd_5. (b) Ca and Cu coordination environments in $Ca_{10}Cd_{27}Cu_2$ largely resemble those from these binary phases.

of the $Ca_{10}Cd_{27}Cu_2$ composition as a linear combination of $CaCd_2$, $Ca_{14}Cd_{51}$, and Cu_2Cd_5 has structural relevance. At the level of individual polyhedra, the ternary structure appears to be segregated into fragments of these binary phases.

An explanation of the presence of Bergman clusters in this phase now begins to take form. If one were to try to build a structure by fusing $Ca@Ca_4Cd_{12}$ Friauf polyhedra to $Cu@Cd_{12}$ icosahedra, then it would quickly be found that the best and tightest fit is obtained by merging a triangular face of the Friauf polyhedron's Cd_{12} truncated tetrahedron with one of the triangular faces of the icosahedron. If there are many more Ca-centered Friauf polyhedra to work with than Cu-centered icosahedra, as would be expected from the high Ca/Cu ratio in $Ca_{10}Cd_{27}Cu_2$, then it would be natural to place a Friauf polyhedron at every face of the Cu-centered icosahedron. The geometry that results from this process is simply the Bergman cluster.

In other words, the introduction of icosahedra into a system of Friauf polyhedra provides excellent nuclei for Bergman clusters. The $MgZn_2$-type $CaCd_2$ phase provides just such a collection of Friauf polyhedra, and the addition of Cu to move the composition closer to $Ca_{10}Cd_{27}Cu_2$ provides an impetus for icosahedron formation. This tendency is most clearly seen for the Cu1 sites at the centers of the Bergman clusters. However, the Cu2 sites play a similar role: they in fact form the cores of Bergman-like clusters with disordered regions (not shown).

Although this picture is consistent with what is structurally observed, implicit in it are two assumptions that need to be examined more closely: (1) Ca−Cd and Cu−Cd interactions prefer to be segregated from each other spatially and (2) Ca−Cd and Cu−Cd interactions are somehow interdependent, preventing macroscopic phase segregation of the sample into Ca−Cd and Cu−Cd compounds. In the next section, we will see how DFT-CP analysis elucidates the tension between Ca−Cd and Cu−Cd interactions.

3.3. Exploring Frustration with DFT-CP Analysis. In the previous section, we made a connection between the formation of Bergman clusters and the spatial segregation of Ca−Cd and Cu−Cd interactions in $Ca_{10}Cd_{27}Cu_2$. For the remainder of this Article, we will examine the origins of this segregation in chemical bonding. Although electronic structure analysis of the full disordered structure of $Ca_{10}Cd_{27}Cu_2$ is a daunting prospect, much can be learned from the DFT-CP distributions of its nearby binary phases $CaCd_2$ and Cu_2Cd_5. Given this compound's particularly close compositional and structural proximity to $MgZn_2$-type $CaCd_2$, one starting point is to investigate how Cu substitution into $CaCd_2$ affects the favorability of the $MgZn_2$ structure type. To do this, we performed LDA-DFT geometrical optimizations of $CaCd_2$ and Cu-substituted models and then searched for frustrated interactions using the DFT-CP analysis recently developed in our group.[66,67,72]

In this theoretical approach, the total energy of a structure is resolved spatially onto a grid over the structure. Examining how varying the volume of the unit cell changes the energy at each grid point allows a pressure map to be calculated for the structure. The pressure map is then divided into domains for particular interatomic interactions; integration over these domains yields interatomic pressures.

The results of applying this procedure to the $MgZn_2$-type $CaCd_2$ phase are illustrated in Figure 6. Here, the crystal

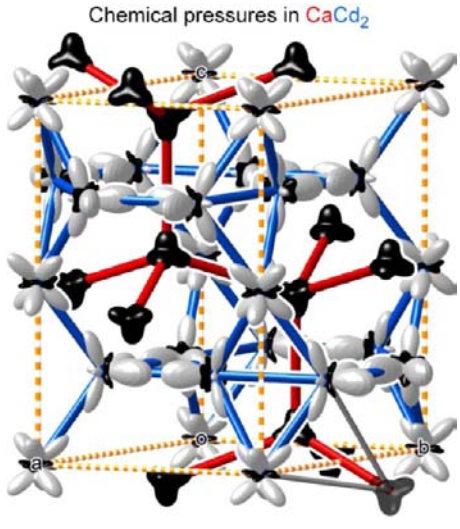

Figure 6. DFT-CP anisotropy surfaces calculated for the $MgZn_2$-type form of $CaCd_2$. On each atom, the pressure experienced along a given direction is represented by a radial plot, with color indicating the sign of the pressure. Black lobes correspond to negative pressures, which call for the contraction of the structure (recalling the suction of a black hole). White lobes indicate positive pressures, which would be relieved by structural expansion (mimicking the expansive force of a supernova).

dx.doi.org/10.1021/ja407291t | J. Am. Chem. Soc. 2013, 135, 17369−17378

structure is shown with each atomic position overlaid with a surface describing the pressure distribution around that atom. In this plot, the Ca positions are decorated with black (negative pressure) tetrapods whose legs point along the Ca−Ca contacts. This indicates that these contacts are overly long and would benefit energetically from contraction. This is counteracted by positive CPs within the Cd sublattice, the contacts within which are all punctuated by white lobes.

From these results, we see a tension between the desires for shorter Ca−Ca distances and longer Cd−Cd ones. For the Ca−Cd interactions, however, the CP features are more minor. Small black lobes emanate from the Cd surfaces pointing toward the grooves in the black Ca surfaces (gray bars near the lower right corner of Figure 6). The signs of the pressures along these contacts are negative, suggesting that the Ca−Cd bonding would benefit from shorter distances, but the magnitudes are smaller than for Ca−Ca or Cd−Cd interactions. In other words, the heteroatomic interactions are well optimized at the expense of homoatomic ones. Considering that heteroatomic interactions are the primary driving force for binary phase formation, this CP distribution bodes well for the stability of the compound.

Let us now turn to how the incorporation of Cu into this lattice would affect this balance of interactions. Because Cu is more similar to Cd than to Ca in size, electronegativity, and electron configuration, the Cd positions are expected to be the most accommodating for Cu atoms. In Figure 7, we show how the CP distribution at the Ca site is affected when one Cd atom per unit cell is replaced with Cu.

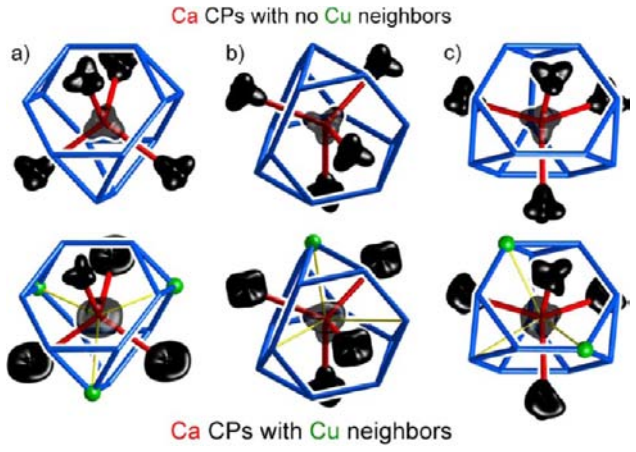

Figure 7. Effect of Cu substitution on the chemical pressures (CPs) experienced by the Ca atoms in the $MgZn_2$-type phase of $CaCd_2$. DFT-CP anisotropy surfaces for Ca atoms in $CaCd_2$ are plotted above those with Cu atoms (green spheres) placed in their coordination environments at (a) Cd1 or (b, c) Cd2 positions. (See Figure S3 for more detailed views.) Yellow lines: contacts with the greatest increase in CP after Cu substitution. Plotting conventions are given in the caption to Figure 6.

We begin in Figure 7a with Cu substitution at the Cd1 site. Because of the relatively small size of the unit cell along *a* and *b*, placing a single Cu atom per unit cell here corresponds to creating a triangle of Cu atoms around the Ca atoms in the same layer of Friauf polyhedra. Because Cu atoms are smaller than Cd atoms, the Ca would be expected to desire shorter contacts to the Cu than to the Cd. However, the triangular arrangement of Cu atoms prevents the Ca from migrating toward one Cu without lengthening another Ca−Cu contact. In the CP anisotropy surfaces, this results in an expansion of the negative CP features along the Ca−Cu contacts. In these directions, the indentations of the CP surface evident in $CaCd_2$ have vanished. Instead, a broad disc appears in the plane of the Ca−Cu contacts.

Similar results are obtained for Cu substitution on the Cd2 site. When one Cd2 site/cell is occupied by Cu, two symmetry-distinct Ca atoms with Cu neighbors result. For one of these Ca sites, a single Cu atom is present in the surrounding Cd/Cu truncated tetrahedron (Figure 7b). For the other, two Cu atoms sit on opposite sides of the same hexagonal face (Figure 7c). In both cases, the Ca CP anisotropy surfaces are significantly expanded along certain directions relative to those of $CaCd_2$.

What is driving the increased negative pressure around the Ca atoms? As a guide to the eye, in Figure 7 we have added yellow bars passing from the central Ca atom toward the atoms outside the inflated regions of the CP surface. These bars, then, trace out the contacts whose distances have become substantially less ideal following Cu substitution into the structure. For both Ca atoms with Cu atoms on Cd2 sites, some yellow lines lie along Ca−Cd contacts that point away from the Ca−Cu ones. As an analysis of the distances around the Ca atoms confirms, the increased negative pressure emerges as the Ca atoms move toward the smaller Cu atoms. The positive pressures within the Cd/Cu sublattice prevent the Cd atoms from effectively following Ca as it moves closer to the Cu atoms. Increased negative pressures are also evident in the figure along the too-long Ca−Cu contacts (but this feature is more dependent on the details of the theoretical treatment).

Both Cu substitution patterns illustrated in Figure 7 point to frustration arising from the addition of Cu to a $CaCd_2$ $MgZn_2$-type phase. In $CaCd_2$, positive pressures between the Cd atoms constrain the contraction of Ca−Ca and to lesser extent Ca−Cd interatomic contacts. The result is the concentration of negative pressure around the Ca atoms. When some of the Cd atoms are replaced with smaller Cu ones, the positive pressures within the Cd/Cu sublattice prevent the coordination environments of Ca from shrinking.

These results can be understood from the point of view of the classic sphere-packing model of the Laves phases.[73−75] Recall that the $MgZn_2$ type is a binary structure type well adapted to pairs of elements with two very different atomic sizes. With the right radius ratio, perfect sphere contacts can be achieved with larger atoms at the Mg positions and smaller ones at the Zn positions. The Ca−Cd−Cu combination, however, is a poor approximation to a binary system: the large difference in metallic radius between Cd and Cu (1.51 vs 1.28 Å)[76] suggests that they would have difficulty satisfying their bonding requirements simultaneously while sharing the same sites within a structure.

3.4. Interdependence of Ca−Cd and Cu−Cd Bonding.

An open question, however, is why the structure should undergo such extreme rearrangements to accommodate both Ca and Cu in the same Cd sublattice when macroscopic phase segregation would seem to be a simpler solution. The answer to this question can be found in the DFT-CP distributions of the closest Cu−Cd binary phase in the Ca−Cd−Cu phase diagram: Cu_2Cd_5. Its crystal structure is based on a network of face-sharing Cd octahedra that traces out the hexagonal diamond structure (blue, Figure 8). Cu atoms fit into the two types of polyhedra (green) offered by voids of the Cd framework:

dx.doi.org/10.1021/ja407291t | J. Am. Chem. Soc. 2013, 135, 17369−17378

tricapped trigonal prisms and partial icosahedra completed by neighboring Cu atoms.

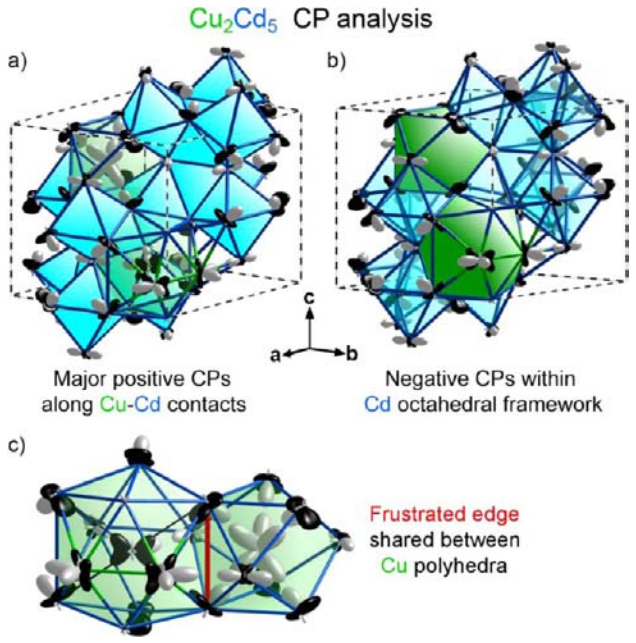

Figure 8. DFT-CP anisotropy surfaces calculated for Cu_2Cd_5 (Co_2Al_5 type). To aid in the visualization of the CP surfaces, the structure is shown with (a) the Cu coordination polyhedra transparent and the Cd octahedra opaque and (b) vice versa. For clarity, only one instance of each symmetry-independent Cu-centered polyhedron is shown. A key factor here is (c) a conflict along edges shared between Cu-centered polyhedra. Refer to Figure 6 for plotting conventions.

Figure 8a focuses on the CP distribution surrounding the Cu atoms, with the Cu-centered polyhedra shown as transparent against a background of solid Cd octahedra. One of the tricapped trigonal prisms is shown in the upper right, where six relatively large, white positive-pressure lobes point from the Cu to the Cd atoms above and below it. This outward pressure on its environment suggests that the Cu atom is relatively large for this space in the structure.

A more complicated CP scheme is seen for the icosahedral Cu site. Similar positive pressure protrusions can be seen pointing from the central Cu atom to two of its Cd neighbors at the back of the polyhedron. However, there are also negative-pressure features on the Cu atom's CP anisotropy surface: four black lobes stretch out from the Cu atom in a plane nearly parallel to the page. The four lobes resemble the corners of a bowtie and point along Cu−Cd contacts. Averaging over the Cu CP anisotropy surface indicates that the positive CP lobes win out: the net CP for these sites comes out to be +24.6 GPa.

Curiously, even the Cu−Cd negative-pressure features can be linked to the positive-pressure repulsion between these two elements in this structure. This connection arises from the sharing of vertices between the two types of Cu polyhedra, as is shown in Figure 8c. At certain shared edges (red), the positive CP within the tricapped trigonal prism calls for lengthening of the edges. This leads to unusually long distances from the affected Cd atoms to the central Cu atom of 3.00 Å (in the DFT optimized geometry). The negative CP lobes on the icosahedral Cu result from these overly extended contacts.

The Cu−Cd contacts within the Cu-centered icosahedra are not the only ones coping with the positive pressures of the tricapped trigonal prisms. Figure 8b focuses on the CP distribution in the Cd sublattice using transparent polyhedral faces for the Cd octahedra. The features between the Cd atoms of the octahedral network are relatively small in magnitude, but a close inspection reveals that they are predominantly negative. The Cd sublattice as a whole desires the contraction of the lattice. As such, it can be viewed as a negative-pressure matrix that the Cu atoms push against.

We are now in a position from which the favorability of combining Cu−Cd and Ca−Cd interactions, as in $Ca_{10}Cd_{27}Cu_2$, begins to be evident. This is illustrated in Figure 9, where we overlay our DFT-CP results for $CaCd_2$ and

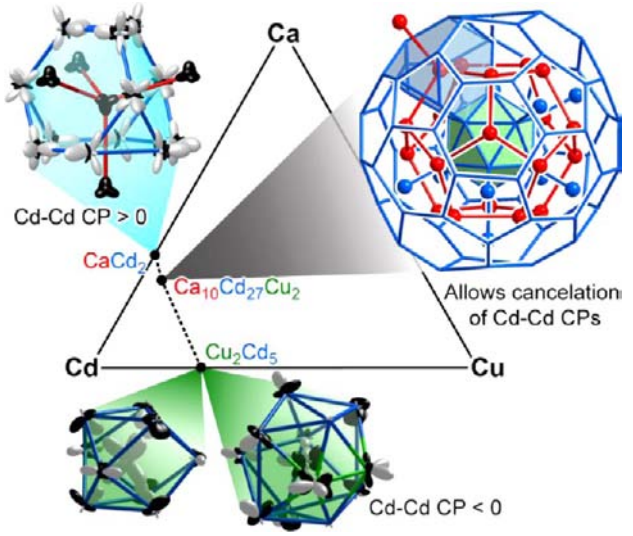

Figure 9. Driving force for ternary phase formation at compositions intermediate between $CaCd_2$ and Cu_2Cd_5. The pressures within the Cd frameworks are of opposite sign in these binaries: positive for $CaCd_2$ and negative for Cu_2Cd_5. Nesting a $Cu@Cd_{12}$ icosahedron in the center of the Bergman cluster built from Ca−Cd Friauf polyhedra could allow for the cancellation of these effects. See Figure 6 for plotting conventions.

Cu_2Cd_5, and the structure of a Bergman cluster (representing $Ca_{10}Cd_{27}Cu_2$) on the ternary composition space of the Ca−Cd−Cu phase diagram. For $CaCd_2$, negative CPs along the Ca−Cd and Ca−Ca contacts force positive pressures to form within the Cd sublattice. For Cu_2Cd_5, the placement of positive and negative CPs within the structure is almost reversed: interactions within the Cd sublattice (as well as some Cu−Cd contacts) experience negative CP as they accommodate Cu atoms, which appear to be relatively large in their structural and electronic context. Combining Ca−Cd and Cu−Cd interactions could allow these pressures of opposite sign to cancel.

This possibility can be seen in the structure of the Bergman cluster. The Ca−Cd and Ca−Ca interactions tend to force overly short contacts between Cd atoms, and this could be expected to compress the central icosahedron of the Bergman cluster as well. The placement of a Cu atom in the center of the cluster would lead to the expansion of the icosahedron and the relief of positive pressures between the surrounding Cd atoms. Our preliminary calculations on a 1/1 Bergman approximant tend to support this view, which we plan to present alongside more detailed calculations on the full $Ca_{10}Cd_{27}Cu_2$ structure in a future publication.

dx.doi.org/10.1021/ja407291t | J. Am. Chem. Soc. 2013, 135, 17369−17378

The interplay of interactions envisioned here for the Bergman clusters of $Ca_{10}Cd_{27}Cu_2$ can be concisely summarized with an analogy to micelles. For amphiphilic molecules, with their incompatible domains (e.g. hydrophilic and hydrophobic), the typical macroscopic phase segregation into two bonding types is prevented by covalent linkages. Under certain conditions, the greatest stability is provided by the aggregation of the molecules into micelles, globules with hydrophobic cores and hydrophilic shells.[43] The Ca−Cd−Cu system exhibits parallel features. There is a similar desire for segregation, this time between Ca−Cd and Cu−Cd interactions. However, unlike covalent linkages in the case of amphiphiles, here the opportunity for the cancellation of opposite chemical pressure effects at the interfaces between these bonding types ties them together. The Bergman cluster plays a similar role to that of the micelle in balancing competing interactions.

4. CONCLUSIONS

We were originally drawn to the Ca−Cd−Cu ternary system by an interest in how competing preferences between the binary combinations of the elements might be reconciled structurally in a ternary phase. Throughout the synthesis, structure determination, and theoretical analysis of $Ca_{10}Cd_{27}Cu_2$ described in this Article, the theme of chemical frustration has been overarching. $Ca_{10}Cd_{27}Cu_2$ crystallizes in an unprecedented monoclinic variation on the 1/1 Bergman approximant structure type, in which [110] layers of this structure are exfoliated through the insertion of additional atoms. The interstitial nature of the space between the Bergman cluster layers is accentuated by its pronounced positional disorder.

Many of the structural features of the compounds can be rationalized by what we call a structure−composition space analysis. In the composition space of the Ca−Cd−Cu phase diagram, $Ca_{10}Cd_{27}Cu_2$ can be represented as a linear combination of the binary formulas corresponding to compounds $CaCd_2$, $Ca_{14}Cd_{51}$, and Cu_2Cd_5. The coordination polyhedra of the ordered Ca and Cu atoms in $Ca_{10}Cd_{27}Cu_2$, built largely from a matrix of Cd atoms, can each be connected to those of these binary phases. In particular, the Bergman clusters can be seen as a core−shell arrangement of a Cu−Cd icosahedron from Cu_2Cd_5 inside an array of Ca−Cd Friauf polyhedra from $CaCd_2$.

The driving force for the formation of the Bergman cluster was investigated using DFT-CP calculations. These calculations showed that a frustration arises when Cu is incorporated into the Cd sublattice of $CaCd_2$, the binary phase closest in composition to $Ca_{10}Cd_{27}Cu_2$. Phase segregation into binaries $CaCd_2$ and Cu_2Cd_5 offers a better alternative to Cu-substituted $CaCd_2$. However, the encapsulation of Cu into the center of a Ca−Cd Bergman cluster could allow the opposite stresses in the Cd sublattices of $CaCd_2$ and Cu_2Cd_5 to negate each other partially, stabilizing the ternary phase. The core−shell segregation of bonding types recalls that of micelles formed from amphiphilic molecules.

The emerging picture of the origins of $Ca_{10}Cd_{27}Cu_2$ in the complementary chemical pressure schemes of the nearby binary phases suggests a strategy for the design of new intermetallic compounds. One can imagine constructing ternary combinations of the form $A_{1-x}B_xC_y$ ($y \gg 1$), where A−C phases show positive CPs within the C sublattice and B−C phases exhibit negative CPs between the C atoms. Synthesis within this system could then reveal phases in which the interfaces between $A@C_n$ and $B@C_{n'}$ polyhedra are stabilized by CP release. We are already exploring this approach through the theoretical analysis of other phases that we have encountered in our search for chemical frustration at work in intermetallics and are looking forward to testing it as the basis for future synthetic endeavors.

■ ASSOCIATED CONTENT

Supporting Information

Powder diffraction data and additional crystallographic refinement procedures for $Ca_{10}Cd_{27}Cu_2$. Refined atomic coordinates, displacement parameters, and selected interatomic distances. Detailed computational procedures and considerations. This material is available free of charge via the Internet at http://pubs.acs.org.

■ AUTHOR INFORMATION

Corresponding Author

danny@chem.wisc.edu

Notes

The authors declare no competing financial interest.

■ ACKNOWLEDGMENTS

We thank Joshua Engelkemier and Veronica Berns for helpful discussions regarding the DFT-CP analysis. We are grateful to Dr. Ilia Guzei for assistance with collecting and processing single-crystal X-ray diffraction data obtained on the Bruker Quazar APEX2 system. We also gratefully acknowledge financial support from the Department of Energy, Office of Science, Early Career Research Program (DE-SC0003947), through the Office of Basic Energy Sciences. This research involved calculations using computer resources supported by National Science Foundation grant CHE-0840494.

■ REFERENCES

(1) *Quasicrystals: An Introduction to Structure, Physical Properties, and Applications*; Suck, J.-B., Schreiber, M., Haussler, P., Eds.; Springer: Berlin, 2002.
(2) Shechtman, D.; Blech, I.; Gratias, D.; Cahn, J. W. *Phys. Rev. Lett.* **1984**, *53*, 1951−1953.
(3) Janssen, T. *Acta Crystallogr., Sect. A* **1986**, *42*, 261−271.
(4) Steurer, W.; Kuo, K. H. *Acta Crystallogr., Sect. B* **1990**, *46*, 703−712.
(5) Yamamoto, A.; Kato, K.; Shibuya, T.; Takeuchi, S. *Phys. Rev. Lett.* **1990**, *65*, 1603−1606.
(6) Yamamoto, A. *Acta Crystallogr., Sect. A* **1996**, *52*, 509−560.
(7) Takakura, H.; Gomez, C. P.; Yamamoto, A.; De Boissieu, M.; Tsai, A. P. *Nature Mater.* **2007**, *6*, 58−63.
(8) Zeng, X. B.; Ungar, G.; Liu, Y. S.; Percec, V.; Dulcey, S. E.; Hobbs, J. K. *Nature* **2004**, *428*, 157−160.
(9) Hayashida, K.; Dotera, T.; Takano, A.; Matsushita, Y. *Phys. Rev. Lett.* **2007**, *98*, 195502.
(10) Lee, S.; Bluemle, M. J.; Bates, F. S. *Science* **2010**, *330*, 349−353.
(11) Fischer, S.; Exner, A.; Zielske, K.; Perlich, J.; Deloudi, S.; Steurer, W.; Lindner, P.; Forster, S. *Proc. Natl. Acad. Sci. U.S.A.* **2011**, *108*, 1810−1814.
(12) Talapin, D. V.; Shevchenko, E. V.; Bodnarchuk, M. I.; Ye, X. C.; Chen, J.; Murray, C. B. *Nature* **2009**, *461*, 964−967.
(13) Dzugutov, M. *Phys. Rev. Lett.* **1993**, *70*, 2924−2927.
(14) Keys, A. S.; Glotzer, S. C. *Phys. Rev. Lett.* **2007**, *99*, 235503.
(15) Zhou, Z. F.; Harris, K. D. M. *ChemPhysChem* **2006**, *7*, 1649−1653.
(16) Zhou, Z. F.; Harris, K. D. M. *J. Phys. Chem. C* **2008**, *112*, 16186−16188.

(17) Iacovella, C. R.; Keys, A. S.; Glotzer, S. C. *Proc. Natl. Acad. Sci. U.S.A.* **2011**, *108*, 20935−20940.
(18) Steurer, W. *Chem. Soc. Rev.* **2012**, *41*, 6719−6729.
(19) Tsai, A. P.; Inoue, A.; Yokoyama, Y.; Masumoto, T. *Mater. Trans., JIM* **1990**, *31*, 98−103.
(20) Mizutani, U.; Takeuchi, T.; Fournee, V.; Sato, H.; Banno, E.; Onogi, T. *Scr. Mater.* **2001**, *44*, 1181−1185.
(21) Mizutani, U.; Takeuchi, T.; Sato, H. *J. Non-Cryst. Solids* **2004**, *334*, 331−335.
(22) Tsai, A. P. *J. Non-Cryst. Solids* **2004**, *334*, 317−322.
(23) Mizutani, U. *Hume-Rothery Rules for Structurally Complex Alloy Phases*; CRC Press: Boca Raton, FL, 2011.
(24) Smith, A. P.; Ashcroft, N. W. *Phys. Rev. Lett.* **1987**, *59*, 1365−1368.
(25) Fujiwara, T. *Phys. Rev. B* **1989**, *40*, 942−946.
(26) Lee, C. S.; Miller, G. J. *J. Am. Chem. Soc.* **2000**, *122*, 4937−4947.
(27) Lin, Q. S.; Corbett, J. D. *Inorg. Chem.* **2004**, *43*, 1912−1919.
(28) Lin, Q. S.; Corbett, J. D. *J. Am. Chem. Soc.* **2005**, *127*, 12786−12787.
(29) Lin, Q.; Corbett, J. D. *Philos. Mag.* **2006**, *86*, 607−613.
(30) Lin, Q. S.; Corbett, J. D. *Struct. Bonding (Berlin)* **2009**, *133*, 1−39.
(31) Takeuchi, T.; Mizutani, U. *Phys. Rev. B* **1995**, *52*, 9300−9309.
(32) Ishii, Y.; Fujiwara, T. *Phys. Rev. Lett.* **2001**, *87*, 206408.
(33) Wu, L. M.; Seo, D. K. *J. Am. Chem. Soc.* **2004**, *126*, 4398−4403.
(34) Andersson, S.; Hyde, S. T.; von Schnering, H. G. *Z. Kristallogr.* **1984**, *168*, 1−17.
(35) Hyde, S. T.; Andersson, S. *Z. Kristallogr.* **1985**, *170*, 225−239.
(36) Nesper, R.; von Schnering, H. G. *Angew. Chem., Int. Ed.* **1986**, *25*, 110−112.
(37) von Schnering, H. G.; Nesper, R. *Angew. Chem., Int. Ed.* **1987**, *26*, 1059−1080.
(38) von Schnering, H. G.; Nesper, R. *Z. Phys. B: Condens. Matter* **1991**, *83*, 407−412.
(39) Hyde, S.; Andersson, S.; Larsson, K.; Blum, Z.; Landh, T.; Lidin, S.; Ninham, B. W. *The Language of Shape*; Elsevier: Amsterdam, 1997.
(40) Grin, Y.; Wedig, U.; von Schnering, H. G. *Angew. Chem., Int. Ed.* **1995**, *34*, 1204−1206.
(41) Fredrickson, D. C.; Lee, S.; Hoffmann, R. *Angew. Chem., Int. Ed.* **2007**, *46*, 1958−1976.
(42) Bates, F. S.; Fredrickson, G. H. *Annu. Rev. Phys. Chem.* **1990**, *41*, 525−557.
(43) Hamley, I. W. *The Physics of Block Copolymers*; Oxford University Press: Oxford, U.K., 1998.
(44) Harris, N. A.; Hadler, A. B.; Fredrickson, D. C. *Z. Anorg. Allg. Chem.* **2011**, *637*, 1961−1974.
(45) Hadler, A. B.; Fredrickson, D. C. *J. Am. Chem. Soc.* **2012**, *134*, 10361−10364.
(46) Bergman, G.; Waugh, J. L. T.; Pauling, L. *Acta Crystallogr.* **1957**, *10*, 254−258.
(47) Tsai, A. P.; Guo, J. Q.; Abe, E.; Takakura, H.; Sato, T. J. *Nature* **2000**, *408*, 537−538.
(48) Bruzzone, G. *Gazz. Chim. Ital.* **1972**, *102*, 234−242.
(49) Gomez, C. P.; Lidin, S. *Angew. Chem., Int. Ed.* **2001**, *40*, 4037−4039.
(50) *CrysAlisPro Software System*; Agilent Technologies.
(51) *APEX2*, version 2013.6-2; Bruker-AXS: Madison, WI, 2013.
(52) Sheldrick, G. M. *XPREP*, version 2013/1. Georg-August-Universität Göttingen: Göttingen, Germany, 2013.
(53) *SADABS*, version 2012/1; Bruker-AXS: Madison, WI, 2012.
(54) Oszlányi, G.; Sütő, A. *Acta Crystallogr., Sect. A* **2004**, *60*, 134−141.
(55) Oszlányi, G.; Sütő, A. *Acta Crystallogr., Sect. A* **2005**, *61*, 147−152.
(56) Palatinus, L.; Chapuis, G. *J. Appl. Crystallogr.* **2007**, *40*, 786−790.
(57) Petříček, V.; Dušek, M.; Palatinus, L. *Jana2006*; The Crystallographic Computing System, Institute of Physics: Praha, Czech Republic, 2006.
(58) Momma, K.; Izumi, F. *J. Appl. Crystallogr.* **2008**, *41*, 653−658.
(59) Goedecker, S.; Teter, M.; Hutter, J. *Phys. Rev. B* **1996**, *54*, 1703−1710.
(60) Hartwigsen, C.; Goedecker, S.; Hutter, J. *Phys. Rev. B* **1998**, *58*, 3641−3662.
(61) Gonze, X.; Rignanese, G. M.; Verstraete, M.; Beuken, J. M.; Pouillon, Y.; Caracas, R.; Jollet, F.; Torrent, M.; Zerah, G.; Mikami, M.; Ghosez, P.; Veithen, M.; Raty, J. Y.; V, O.; Bruneval, F.; Reining, L.; Godby, R.; Onida, G.; Hamann, D. R.; Allan, D. C. *Z. Kristallogr.* **2005**, *220*, 558−562.
(62) Gonze, X.; Amadon, B.; Anglade, P. M.; Beuken, J. M.; Bottin, F.; Boulanger, P.; Bruneval, F.; Caliste, D.; Caracas, R.; Cote, M.; Deutsch, T.; Genovese, L.; Ghosez, P.; Giantomassi, M.; Goedecker, S.; Hamann, D. R.; Hermet, P.; Jollet, F.; Jomard, G.; Leroux, S.; Mancini, M.; Mazevet, S.; Oliveira, M. J. T.; Onida, G.; Pouillon, Y.; Rangel, T.; Rignanese, G. M.; Sangalli, D.; Shaltaf, R.; Torrent, M.; Verstraete, M. J.; Zerah, G.; Zwanziger, J. W. *Comput. Phys. Commun.* **2009**, *180*, 2582−2615.
(63) Vanderbilt, D. *Phys. Rev. B* **1990**, *41*, 7892−7895.
(64) Kresse, G.; Furthmüller, J. *Phys. Rev. B* **1996**, *54*, 11169−11186.
(65) Kresse, G.; Furthmüller, J. *Comput. Mater. Sci.* **1996**, *6*, 15−50.
(66) Fredrickson, D. C. *J. Am. Chem. Soc.* **2012**, *134*, 5991−5999.
(67) Engelkemier, J.; Berns, V. M.; Fredrickson, D. C. *J. Chem. Theory Comput.* **2013**, *9*, 3170−3180.
(68) Li, B.; Corbett, J. D. *Inorg. Chem.* **2004**, *43*, 3582−3587.
(69) Misch, L. *Metallwirtschaft* **1935**, *14*, 897−899.
(70) Nowotny, H. N. *Z. Metallkd.* **1946**, *37*, 31−34.
(71) Rajasekharan, T.; Schubert, K. *Z. Metallkd.* **1982**, *73*, 262−264.
(72) Fredrickson, D. C. *J. Am. Chem. Soc.* **2011**, *133*, 10070−10073.
(73) Frank, F. C.; Kasper, J. S. *Acta Crystallogr.* **1958**, *11*, 184−190.
(74) Frank, F. C.; Kasper, J. S. *Acta Crystallogr.* **1959**, *12*, 483−499.
(75) Müller, U. *Inorganic Structural Chemistry*; John Wiley & Sons: Chichester, U.K., 2007.
(76) Greenwood, N. N.; Earnshaw, A. *Chemistry of the Elements*, 2nd ed.; Butterworth-Heinemann: Oxford, U.K., 1997.